^{18}F-Labeled Somatostatin Analogs as PET Tracers for the Somatostatin Receptor: Ready for Clinical Use

Hannes Leupe[1], Stephen Ahenkorah[2], Jeroen Dekervel[3], Marcus Unterrainer[4,5], Eric Van Cutsem[3], Chris Verslype[3], Frederik Cleeren[2], and Christophe M. Deroose[1]

[1]Nuclear Medicine, University Hospitals Leuven, and Nuclear Medicine and Molecular Imaging, Department of Imaging and Pathology, University of Leuven, Leuven, Belgium; [2]Radiopharmaceutical Research, Department of Pharmacy and Pharmacology, University of Leuven, Leuven, Belgium; [3]Digestive Oncology, University Hospitals Leuven, Leuven, Belgium; [4]Department of Radiology, University Hospital, LMU Munich, Munich, Germany; and [5]Department of Nuclear Medicine, University Hospital, LMU Munich, Munich, Germany

Molecular imaging of the somatostatin receptor plays a key role in the clinical management of neuroendocrine tumors. PET imaging with somatostatin analogs (SSAs) labeled with ^{68}Ga or ^{64}Cu is currently the gold standard in clinical practice. However, widespread implementation of ^{68}Ga imaging is often hampered by practical and economic issues related to ^{68}Ge/^{68}Ga generators. ^{18}F offers several advantages to tackle these issues. Recent developments in radiochemistry have allowed a shift from ^{68}Ga toward ^{18}F labeling, leading to promising clinical translations of ^{18}F-labeled SSAs, such as Gluc-Lys-[^{18}F]FP-TOCA, [^{18}F]F-FET-βAG-TOCA, [^{18}F]AlF-NOTA-octreotide, [^{18}F]SiTATE, and [^{18}F]AlF-NOTA-JR11. This review gives an update of currently available clinical data regarding ^{18}F-labeled SSA tracers and provides justification for the clinical application of this class of tracers.

Key Words: neuroendocrine; radiopharmaceuticals; fluorine-18-labeled PET tracer; neuroendocrine tumor; somatostatin analogue; somatostatin receptor

J Nucl Med 2023; 64:835–841
DOI: 10.2967/jnumed.123.265622

Neuroendocrine tumors (NETs) are a heterogeneous group of tumors derived from cells of the diffuse neuroendocrine system. They are most commonly found in the gastrointestinal tract or respiratory system and can secrete various hormones, giving rise to a wide range of clinical symptoms. Although typically described as rare, the incidence of NETs has increased steadily over the past 40 y, with a currently estimated incidence of 5 per 100,000 persons per year (*1*).

Most differentiated NETs are characterized by an overexpression of the somatostatin receptor (SSTR), a G-protein–coupled membrane receptor (*2*). Five different human SSTR subtypes have been identified: 1, 2A/2B, 3, 4, and 5. For subtype 5, truncated splice variants have been described in NETs (*3*). SSTRs are expressed by a wide variety of normal human tissues, each exhibiting a characteristic expression pattern of the different SSTR subtypes (*4*). SSTRs have also been identified in several human tumor types, with NETs representing one of the groups with the highest incidence of SSTR expression (*5*). For example, SSTRs are present in 80%–100% of gastroenteropancreatic NETs, and most gastroenteropancreatic NETs have moderate-to-high overexpression of SSTRs, especially subtype 2A (*6*). SSTR overexpression is also seen in other NETs, such as pheochromocytomas, paragangliomas, small-cell lung cancers, lung carcinoids, pituitary adenomas, Merkel cell carcinomas, neuroblastomas, and medullary thyroid carcinomas (*7*). However, SSTR expression in tumors is not limited to NETs and can also be found in a large variety of other solid and hematologic malignancies (*8*).

The overexpression of SSTRs on NETs is the foundation on which treatment with somatostatin analogs (SSAs) is based. Moreover, SSAs can be labeled with radionuclides, allowing for imaging or therapy (*2*). These peptide-based radiopharmaceuticals typically consist of the biologically active synthetic peptide (the vector molecule), linked to the radionuclide by means of a chelator (*9*). SSTR imaging was first performed in 1989 using ^{123}I-Tyr^3-octreotide scintigraphy (*10*). ^{123}I was quickly replaced by ^{111}In because of several practical disadvantages such as limited availability, high cost, and suboptimal image quality due to pronounced intestinal accumulation (*11*). [^{111}In]In-DTPA-octreotide (or [^{111}In]In-pentetreotide) SPECT imaging with or without CT has been successfully used for over 2 decades for staging and therapy selection for NETs (*12*). However, the use of ^{111}In was also hampered by several disadvantages, such as unfavorable nuclear physical characteristics resulting in suboptimal image quality and a relatively high radiation burden, limited availability, and high costs (*13*). In the early 2000 s, successful developments were made to label SSAs with ^{99m}Tc (e.g., ^{99m}Tc-EDDA/HYNICTOC), showing higher target-to-background ratios and higher tumor uptake values, which improved image quality (*14*).

A major advancement was the development of SSAs labeled with the positron-emitting radionuclide ^{68}Ga, allowing for PET imaging of SSTR. This was made possible by the chelation of ^{68}Ga by DOTA, which can be coupled to SSAs. Since the introduction of [^{68}Ga]Ga-DOTA SSAs, their superiority over conventional SPECT imaging has been well established, making them the current gold standard for evaluation of SSTR in NETs (*15*). ^{68}Ga-based tracers currently used in clinical practice are [^{68}Ga]Ga-DOTATOC, [^{68}Ga]Ga-DOTATATE, and [^{68}Ga]Ga-DOTANOC. Despite the excellent results achieved with [^{68}Ga]Ga-DOTA SSAs, their use in routine clinical practice is often hampered by practical and economic issues related to ^{68}Ge/^{68}Ga-generators. Disadvantages include high costs, limited

Received Feb. 20, 2023; revision accepted Mar. 24, 2023.
For correspondence or reprints, contact Christophe M. Deroose (christophe.deroose@uzleuven.be).
Published online May 11, 2023.

TABLE 1
Direct Comparison of Pharmacokinetic and Practical Properties of ^{68}Ga, ^{18}F, and ^{64}Cu (*45*)

Property	^{68}Ga	^{18}F	^{64}Cu
Half-life	67.6 min	109.8 min	12.7 h
Production yield/batch	2–4 patients	>10 patients, up to 50	>10 patients, up to 50
Positron energy (E_{max})	1,899 keV	634 keV	653 keV
Average positron range in H_2O	3.5 mm	0.6 mm	0.7 mm
Branching ratio	89.1%	96.9%	17.5%
Source	^{68}Ge/^{68}Ga-generator/cyclotron (solid target)	Cyclotron (liquid target)	Cyclotron (solid target)
Central production	No, if generator-based	Yes	Yes

availability, short tracer half-life (68 min), low production yield (2–4 patients per batch), regulatory or reimbursement barriers, and a relatively high average positron energy (0.83 MeV) with a resulting long average positron range (3.5 mm), possibly compromising spatial resolution (Table 1) (*16*).

Another frequently used radionuclide for SSTR PET imaging is ^{64}Cu. Its half-life (12.7 h) allows for centralized production and a more flexible scanning window. Moreover, its low average positron energy (0.28 MeV) with a corresponding short average positron range (0.8 mm) makes high-spatial-resolution PET imaging possible (*16*). Disadvantages are the low branching ratio—only 17.5%—for positron emission decay and a higher radiation exposure.

^{18}F, by far the most widely used PET radionuclide, offers several advantages including a high production yield (50 patients or more per batch) and a more favorable half-life (109.8 min). These properties allow for centralized production and distribution to distant PET centers without an on-site cyclotron. Furthermore, the shorter positron range (0.6 mm) of ^{18}F than of ^{68}Ga and ^{64}Cu could improve the spatial resolution of the acquired PET data. The branching ratio for positrons, 96.9%, is nearly optimal (*16*).

In recent years, several new ^{18}F-based tracers were designed to target SSTR (Fig. 1; Table 2). This article provides an overview of the currently available clinical data regarding SSTR imaging and more specifically of ^{18}F-based tracers targeting SSTR.

^{18}F-LABELED SSA TRACERS

Gluc-Lys-[^{18}F]FP-TOCA

In 2006, Meisetschläger et al. evaluated the clinical use of Gluc-Lys-[^{18}F]FP-TOCA in 25 patients with SSTR-positive tumors seen on conventional ^{111}In-DTPA-octreotide scans (*17*). In a head-to-head comparison of both imaging modalities in 16 of these patients, Gluc-Lys-[^{18}F]FP-TOCA imaging revealed a significantly higher number of lesions (factor of 2.4), indicating diagnostic superiority. Biokinetic evaluation of Gluc-Lys-[^{18}F]FP-TOCA showed a fast and intense tumor accumulation without intracellular trapping, as well as a rapid clearance from blood serum, predominantly through the kidneys but also by hepatobiliary transport. The tumor-to-background ratio was higher for Gluc-Lys-[^{18}F]FP-TOCA than for [^{111}In]In-DTPA-octreotide, which allowed for clear delineation of the liver lesions. Nevertheless, a major obstacle to clinical implementation of Gluc-Lys-[^{18}F]FP-TOCA was its extensive multistep synthesis with limited radiochemical yield (20%–30%) (*17*). Subsequently, only a few clinical studies have been published using Gluc-Lys-[^{18}F]FP-TOCA (*18–20*), and in these trials only a small number of patients were included. Until now, no direct comparison between Gluc-Lys-[^{18}F]FP-TOCA and another SSTR PET tracer has been made. To our knowledge, no further large clinical trials have been performed.

NOTEWORTHY

- ^{18}F-labeled SSAs as PET tracers for SSTR are ready for routine clinical practice.
- ^{18}F-labeled SSA tracers demonstrate higher in vivo stability, higher tumor-to-background ratios, better lesion detection, more beneficial physical properties, a higher production yield, or a more favorable biodistribution than conventional [^{68}Ga]Ga-DOTA SSA PET/CT imaging, indicating suitability for clinical use.
- ^{18}F-labeled SSTR agonist tracers are valid alternatives to SSTR PET. They should be implemented in guidelines and appropriate-use criteria for SSTR PET imaging.

[^{18}F]F-FET-βAG-TOCA

Another ^{18}F tracer targeting SSTR is [^{18}F]F-FET-βAG-TOCA. Dubash et al. assessed the biodistribution and dosimetry of [^{18}F]F-FET-βAG-TOCA in a first in-humans study with 9 NET patients (*21*). [^{18}F]F-FET-βAG-TOCA showed high tumoral uptake and a high tumor-to-background ratio in all organs including the liver, comparable to values reported for [^{68}Ga]Ga-DOTA SSA tracers. Physiologic uptake was observed in the pituitary, salivary glands, and thyroid tissue. Rapid clearance from most organs was found, with both renal and hepatobiliary excretion. As such, the highest absorbed dose was seen in the gallbladder, followed by the spleen, stomach wall, liver, kidneys, and bladder (*21*). In a larger study cohort, Dubash et al. compared [^{18}F]F-FET-βAG-TOCA directly with [^{68}Ga]Ga-DOTATATE in 32 patients (*22*). [^{18}F]F-FET-βAG-TOCA detected more lesions (209/223) than [^{68}Ga]Ga-DOTATATE (197/223), showing a statistically nonsignificant higher overall sensitivity (92.8% vs. 87.5%) in the detection of NET lesions. Moreover, [^{18}F]F-FET-βAG-TOCA detected additional bone and lymph node lesions in 3 of the patients (9.4%). As [^{18}F]F-FET-βAG-TOCA had promising results for lesion detection in NET patients, further developments could lead to the clinical validation of this promising tracer as a potential alternative to [^{68}Ga]Ga-DOTA SSA tracers.

In a recently published proof-of-concept study, the feasibility of SSTR2 imaging as a novel inflammation-specific molecular imaging target was evaluated with [^{18}F]F-FET-βAG-TOCA and

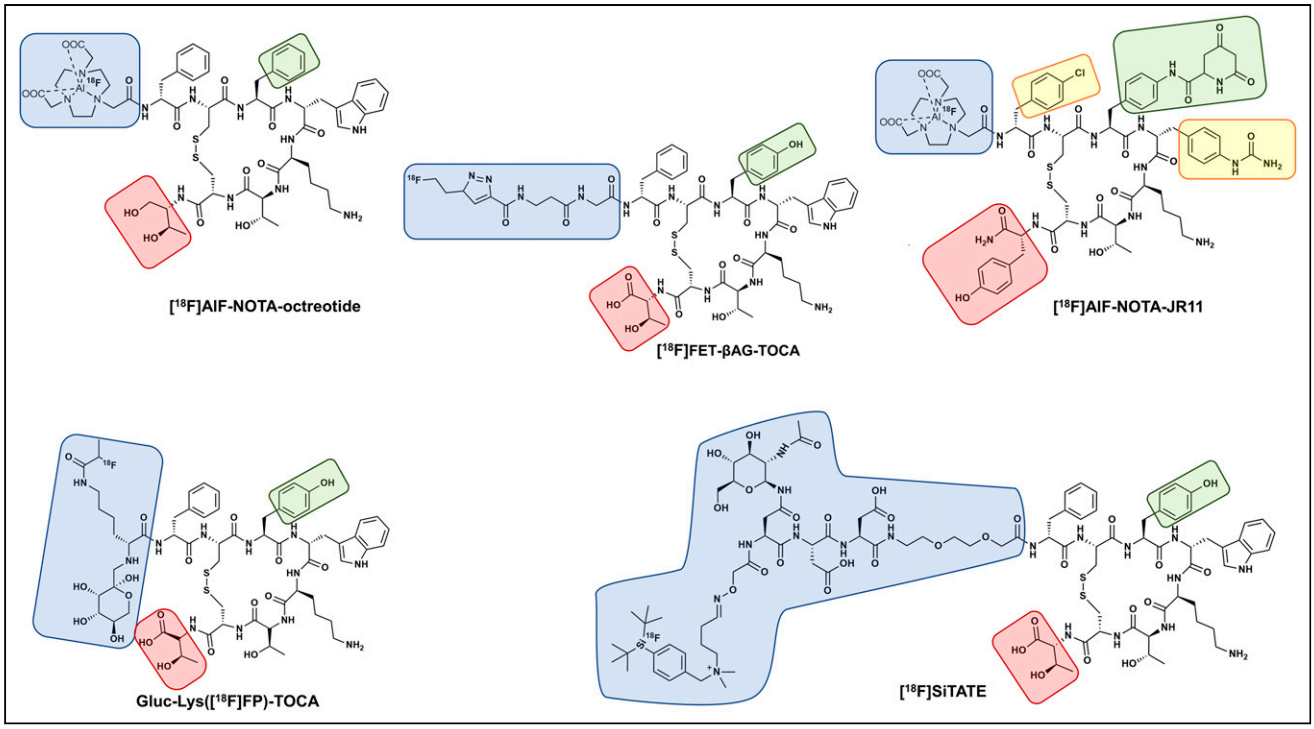

FIGURE 1. Molecular structures of ^{18}F-based SSTR tracers that have been applied in clinical studies.

[^{68}Ga]Ga-DOTATE PET/MR in patients with large-vessel vasculitis. SSTR2 PET/MRI showed major promise for diagnosis and therapeutic monitoring and was generally comparable to [^{18}F]FDG PET/CT, but with a very low background signal in the brain and heart. This allows for better assessment of nearby vascular involvement (*23*).

[^{18}F]AlF-NOTA-Octreotide

Recently, an Al^{18}F-labeled SSTR agonist, [^{18}F]AlF-NOTA-octreotide, was synthesized using a good-manufacturing-practice–compliant, chelator-based, automated radiolabeling method (*24*). In a first in-humans trial by Long et al. on 22 patients with proven NETs, [^{18}F]AlF-NOTA-octreotide PET/CT was directly compared with [^{18}F]FDG PET/CT (*25*). High physiologic uptake was seen in the spleen, kidneys, and bladder, whereas the pituitary, thyroid, adrenal glands, uncinate process of the pancreas, stomach, and intestine also showed mild to moderate physiologic uptake. Brain, lung, muscle, and bone showed a low background activity. The [^{18}F]AlF-NOTA-octreotide PET/CT images showed optimal contrast, with a significantly high tumor-to background ratio. SUV_{max} was higher in well-differentiated NETs than in poorly differentiated tumors. Moreover, lower Ki-67 values were observed in lesions with high [^{18}F]AlF-NOTA-octreotide uptake, and higher [^{18}F]FDG uptake was associated with higher Ki-67 values (*25*). This finding is attributed to a higher metabolic turnover and loss of SSTR expression in high-grade NETs (*6,25*). Hou et al. (*26*) extended the sample size of their previous study (*25*) and evaluated the biodistribution of [^{18}F]AlF-NOTA-octreotide in 128 patients with proven or suspected NETs (*26*). Their analysis confirmed the favorable biodistribution and higher tracer uptake for [^{18}F]AlF-NOTA-octreotide in well-differentiated tumors (G1 or G2) in comparison with G3 lesions, consistent with data from ^{68}Ga-labeled SSTR tracers and in line with lower SSTR expression levels in more aggressive tumors. High tumor-to-background ratios enabled the detection of very small lesions, such as those that are only a few millimeters in size, especially in the lymph nodes and bone. Interestingly, some benign lesions such as thyroid adenoma showed obvious [^{18}F]AlF-NOTA-octreotide uptake, whereas mild to moderate uptake was found in benign lesions such as inflammatory lesions, meningiomas, or fractures, again compatible with uptake patterns observed with ^{68}Ga-labeled SSAs (*26,27*).

After publishing promising results of a direct comparison between [^{18}F]AlF-NOTA-octreotide PET/CT and [^{68}Ga]Ga-DOTATATE in a NET patient (*28*), Pauwels et al. compared both tracers in 6 healthy volunteers and 6 NET patients (*29*). They concluded that [^{18}F]AlF-NOTA-octreotide is safe and well tolerated. The highest dose was received by the spleen, followed by the urinary bladder wall and the kidneys, in accordance with the expected SSTR-specific uptake in the spleen and renal excretion of the tracer. The effective dose was 22.4 ± 4.4 μSv/MBq (*29*).

Generally, both tracers showed a similar physiologic uptake pattern. In comparison with [^{68}Ga]Ga-DOTATATE, most organs, including bone, showed lower uptake for [^{18}F]AlF-NOTA-octreotide PET/CT. Also, liver background uptake was lower for [^{18}F]AlF-NOTA-octreotide, allowing for better liver lesion detection. Moreover, the SUV_{max} for all lesions was significantly lower with [^{18}F]AlF-NOTA-octreotide than with [^{68}Ga]Ga-DOTATATE. However, despite the lower background activity in the bone, [^{18}F]AlF-NOTA-octreotide missed more bone lesions—driven mainly by the results for a single patient (*29*).

In a larger prospective study, Hou et al. compared both tracers in 20 patients with a combined total of 179 lesions and found similar results (*30*). In their analysis, [^{18}F]AlF-NOTA-octreotide showed a 1.5 times lower liver uptake and a 5 times lower uptake in the salivary glands. Both tracers were highly sensitive in lesion detection, with no significant difference in overall diagnostic efficacy.

TABLE 2
Currently Available Clinical Studies on NET or Meningioma Patients Using ^{18}F-Labeled Tracers

Study	Year	*N*	P	^{18}F tracer	Comparator	Outcomes	N_{tot}	N_{tracer} (%)	N_{com} (%)	Main findings
Meisetschläger (*17*)	2006	25	NET	Gluc-Lys-[^{18}F]FP-TOCA	[^{111}In]In-pentetreotide	BD, D, QNA, QLA	—	288	133	ED = 13 μSv/MBq
Seemann (*18*)	2007	31	NET	Gluc-Lys-[^{18}F]FP-TOCA	Triple-phase CT	QLA	1,618	1,519 (93.9)	990 (61.2)	DDR = 32.7%
Wieder (*19*)	2008	10	NET	Gluc-Lys-[^{18}F]FP-TOCA	Triple-phase CT	QNA, QLA	144	139 (96.6)	114 (79.2)	DDR = 17.4%
Astner (*20*)	2009	9	GT	Gluc-Lys-[^{18}F]FP-TOCA	MRI	TD	11	—	—	Improves TD
Dubash (*21*)	2016	9	NET	[^{18}F]F-FET-βAG-TOCA	—	BD, D	—	—	—	ED = 29 μSv/MBq
Dubash (*22*)	2018	32	NET	[^{18}F]F-FET-βAG-TOCA	[^{68}Ga]Ga-DOTATATE	BD, QLA	223	209 (93.7)	197 (88.3)	DDR = 5.4%
Long (*25*)	2019	22	NET	[^{18}F]AlF-NOTA-OC	[^{18}F]FDG	BD, QNA, QLA, D	729	624 (85.6)	390 (53.5)	DDR = 32.1%; ED = 23 μSv/MBq
Hou (*26*)	2021	162	NET	[^{18}F]AlF-NOTA-OC	—	BD, QNA	517	—	—	Similar BD
Pauwels (*28*)	2019	1	NET	[^{18}F]AlF-NOTA-OC	[^{68}Ga]Ga-DOTATATE	QNA	—	—	—	Higher TBR
Pauwels (*29*)	2020	12	NET	[^{18}F]AlF-NOTA-OC	[^{68}Ga]Ga-DOTATATE	BD, D, QLA, QNA	242	218 (90.1)	208 (86.0)	DDR = 4.1%; ED = 22.4 μSv/MBq
Hou (*30*)	2021	20	NET	[^{18}F]AlF-NOTA-OC	[^{68}Ga]Ga-DOTATATE	BD, QLA, QNA	180	177 (98.3)	152 (84.4)	DDR = 13.9%
Pauwels (*31*)	2022	75	NET	[^{18}F]AlF-NOTA-OC	^{68}Ga-labeled SSAs	BD, QLA, QNA	4,709	4,278 (91.1)	3,454 (75.3)	DDR = 15.8%
Haeger (*32*)	2023	20	NET	[^{18}F]AlF-NOTA-OC	[^{68}Ga]Ga-DOTATATE	BD, QLA, QNA	752	747 (99.3)	751 (99.9)	DDR = 0.6%
Ilhan (*36*)	2019	1	NET	[^{18}F]SiTATE	[^{68}Ga]Ga-DOTATOC	BD, QNA	—	—	—	Similar BD and TU
Ilhan (*37*)	2020	13	NET	[^{18}F]SiTATE	[^{68}Ga]Ga-DOTATOC	BD, QNA	109	—	—	Similar BD, higher TU
Beyer (*38*)	2021	8	NET	[^{18}F]SiTATE	[^{68}Ga]Ga-DOTATOC	D, QNA	68	—	—	ED = 15 μSv/MBq
Unterrainer (*40*)	2022	86	M	[^{18}F]SiTATE	CT/MRI	QNA	177	—	—	High TBR
Unterrainer (*41*)	2021	1	M	[^{18}F]SiTATE	[^{68}Ga]Ga-DOTATOC	QNA	1	—	—	Comparable TU
Xie (*43*)	2021	10	NET	[^{18}F]AlF-NOTA-JR11	[^{68}Ga]Ga-DOTATATE	BD, QNA, QLA	227	226 (99.6)	160 (70.5)	DDR = 29.1%

BD = biodistribution; D = dosimetry; DDR = difference in detection rate between tracer and comparator; ED = effective dose studied tracer; GT = skull base glomus tumors; M = meningiomas; N = number of patients; N_{total} = total number of lesions; N_{tracer} = number of lesions detected with ^{18}F tracer; N_{com} = number of lesions detected with comparator tracer; P = study population; QLA = qualitative analysis; QNA = quantitative analysis; TBR = tumor-to-background ratio; TD = target lesion volume delineation); TU = tumor uptake.

However, [^{18}F]AlF-NOTA-octreotide detected more lesions (177 vs. 152; $P = 0.54$), especially lesions in the liver (116 vs. 93; $P < 0.01$), presumably because of the higher tumor-to-background ratio. In contrast to the findings of Pauwels et al. (*29*), the SUV_{max} of [^{18}F]AlF-NOTA-octreotide was higher than that of [^{68}Ga]Ga-DOTATATE, but the difference was not statistically relevant. Interestingly, some patients exhibited higher [^{68}Ga]Ga-DOTATATE uptake in lesions whereas others had higher [^{18}F]AlF-NOTA-octreotide uptake. Moreover, some lesions had higher [^{68}Ga]Ga-DOTATATE uptake whereas others within the same patient had higher [^{18}F]AlF-NOTA-octreotide uptake (*30*).

In a recent prospective, multicenter study, Pauwels et al. compared the diagnostic performance of [^{18}F]AlF-NOTA-octreotide with [^{68}Ga]Ga-DOTATATE or [^{68}Ga]Ga-DOTANOC in 75 patients with histologically confirmed NETs (*31*). With [^{18}F]AlF-NOTA-octreotide, patients underwent whole-body PET 2 h after intravenous injection, whereas conventional PET SSTR imaging is typically done 45–60 min after [^{68}Ga]Ga-DOTA SSA injection. [^{18}F]AlF-NOTA-octreotide detected significantly more lesions (4,278/4,709), with a higher detection rate (91.1%) than [^{68}Ga]Ga-DOTATATE (3,454/4,709; 75.3%), illustrating diagnostic superiority. The detection rate was significantly higher for [^{18}F]AlF-NOTA-octreotide in most organs except for bone lesions, where the difference in detection rate was 2.8%. Although the mean tumor-to-background ratio was significantly higher with [^{18}F]AlF-NOTA-octreotide, no significant differences in mean SUV_{max} were observed. In particular, the lower background uptake with [^{18}F]AlF-NOTA-octreotide resulted in better detection of liver metastases (60.3% vs. 93.3%) (Fig. 2). In accordance with the findings of Hou et al. (*30*), considerable variability in lesion uptake was seen both between and within patients. This can most likely be attributed to tumor heterogeneity and differences in SSTR affinity (*31*). In a recently published prospective trial with 20 NET patients, noninferiority of [^{18}F]AlF-NOTA-octreotide in comparison with [^{68}Ga]Ga-DOTATATE was confirmed (*32*). Differences in lesion detection rate and tumor-to-background ratios were nonsignificant, but [^{18}F]AlF-NOTA-octreotide images showed lower liver and spleen background, providing excellent image quality (*32*).

Besides diagnostic information, [^{18}F]AlF-NOTA-octreotide PET can offer prognostic value in combination with [^{18}F]FDG PET imaging. This was evaluated by Hou et al. in a study of 66 patients with NETs who underwent both imaging modalities (*33*). In this analysis, a visual evaluation method summarizing information from both [^{18}F]FDG and SSTR images (NETPET grading) was further investigated using [^{18}F]AlF-NOTA-octreotide for SSTR imaging. In multivariate analysis, both NETPET grade and SSTR expression (tumor volume multiplied by SUV_{mean}) were independent predictors of progression-free survival (*33*).

[^{18}F]SiTATE

Another promising SSA radiotracer labeled with ^{18}F is [^{18}F]SiTATE, which has shown high selectivity for SSTR2 and can be synthesized in conformation with good manufacturing practices (Fig. 3) (*34,35*). In 2019, the first in-humans [^{18}F]SiTATE PET/CT scan was performed on a patient with metastatic NET and showed cardiac and bone metastasis uptake comparable to that on [^{68}Ga]Ga-DOTATATE PET/CT (*36*). The biodistribution, tumor uptake, and image quality of [^{18}F]SiTATE and [^{68}Ga]Ga-DOTATOC were directly compared in a retrospective study by Ilhan et al. including 13 patients with grade 1 or 2 neuroendocrine neoplasia (*37*). For [^{18}F]SiTATE, physiologic tracer uptake was significantly higher in the kidneys and nonsignificantly higher in the liver, adrenal glands, and spleen. For [^{18}F]SiTATE, a significantly higher tumor uptake was described in almost all tumor lesions in common metastatic sites of NET, including the liver, lymph nodes, and bone, but not in lung lesions. This led to tumor-to-background ratios similar to those for [^{68}Ga]Ga-DOTATOC. One limitation of this study was the relatively large range in time interval between

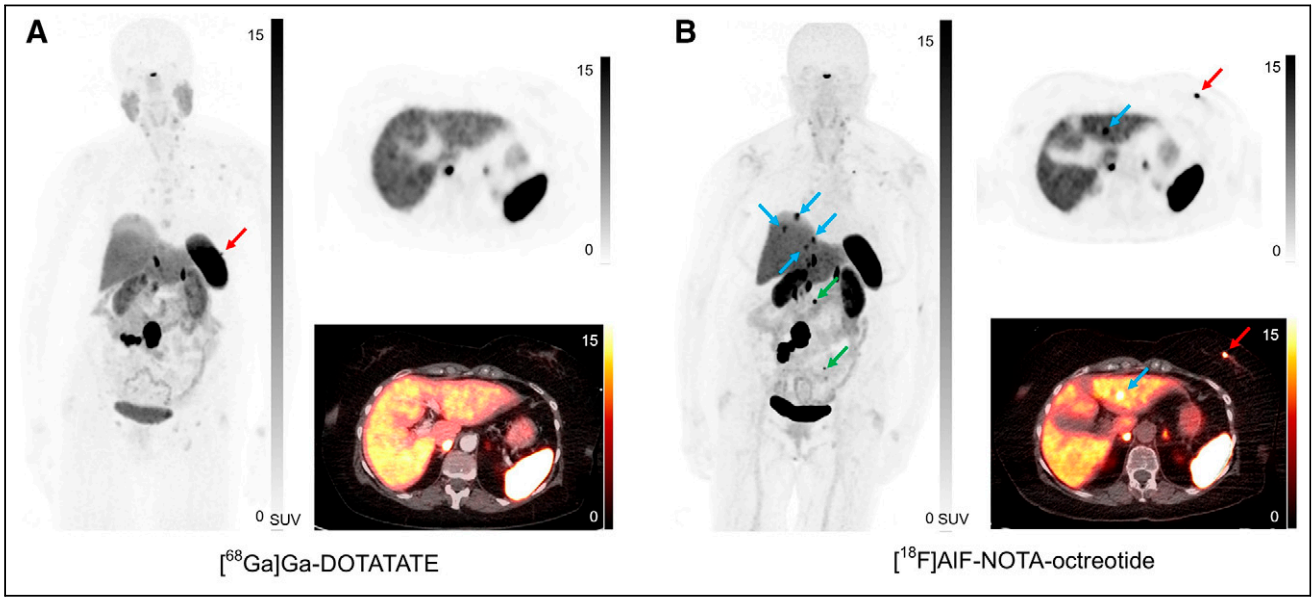

FIGURE 2. [^{68}Ga]Ga-DOTATATE (A) and [^{18}F]AlF-NOTA-octreotide (B) maximum-intensity-projection, PET, and PET/CT images of 69-y-old woman with intestinal NET, multiple liver and lymph node metastases, and 1 breast metastasis. [^{18}F]AlF-NOTA-octreotide PET/CT showed multiple liver lesions (blue arrows), whereas previous [^{68}Ga]Ga-DOTATATE PET/CT (7 d before) showed no liver disease. Furthermore, 2 new lymph node metastases were detected with [^{18}F]AlF-NOTA-octreotide (green arrows). Breast metastasis (red arrow) was also seen on [^{68}Ga]Ga-DOTATATE images but is not depicted on slice shown.

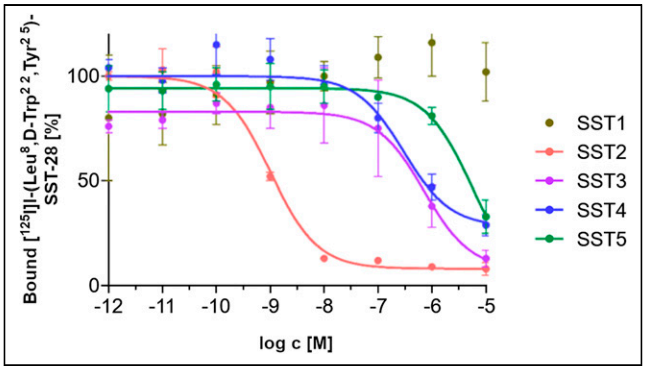

FIGURE 3. In vitro competition experiment using membranes of SSTR subtype–expressing cells. Image shows bound fraction of [^{125}I]I-(Leu^{8}, D-Trp^{22}, Tyr^{25})-SST-28 with increasing concentrations of [^{18}F]SiTATE. [^{18}F]SiTATE shows excellent selectivity for SSTR subtype 2, with only minor affinity to SSTR subtypes 3 and 4. (Reprinted from (*35*).)

the 2 scans (4–26 mo), including heterogeneous therapy options that were applied in between (*37*). Beyer et al. evaluated the biodistribution, optimal scan time, and dosimetry for both tracers in 8 patients and found similar results (*38*). When imaging took place 60 min after injection, tumor-to-background ratios did not significantly differ between [^{68}Ga]Ga-DOTATATE and [^{18}F]SiTATE for most lesions. However, [^{18}F]SiTATE uptake further increased for almost all types of metastases after 60 min, leading to higher tumor-to-background ratios at later scan times. Biodistribution was comparable to [^{68}Ga]Ga-DOTATATE, with bladder and spleen showing the highest radiotracer uptake, followed by kidneys and adrenal glands (*38*). In a recently published study, Eschbach et al. investigated the influence of long-acting SSA medication before [^{18}F]SiTATE on tumor uptake and physiologic uptake (*39*). Similar to ^{68}Ga-labeled SSAs, a significantly lower [^{18}F]SiTATE uptake in normal liver and spleen tissue was observed in patients receiving treatment with long-acting SSAs. However, there was no significant reduction in tumor-to-background ratios, supporting the clinical approach not to discontinue any SSA medication before a PET/CT examination (*39*).

[^{18}F]SiTATE can also be applied for PET imaging of meningiomas. Unterrainer et al. evaluated the feasibility of [^{18}F]SiTATE PET/CT in 86 patients with known or suspected meningioma (*40*). Tracer uptake was very high in meningiomas compared with healthy tissue and nonmeningioma lesions, leading to a high detection of osseous involvement and previously unknown meningioma sites (*40,41*).

[^{18}F]AlF-NOTA-JR11

Noninternalizing SSTR antagonists have the potential to improve SSTR PET/CT imaging because they bind to a greater number of binding sites than agonists, leading to higher tumor accumulation and possibly higher imaging sensitivity. [^{68}Ga]Ga-NODAGA-JR11 has a high affinity for SSTR and is one of the lead molecules for this novel route of SSTR imaging (*42*). In a recent pilot study, Xie et al. compared [^{18}F]AlF-NOTA-JR11, an Al^{18}F-labeled SSTR antagonist, with [^{68}Ga]Ga-DOTATATE in 10 patients with neuroendocrine neoplasia and evaluated biodistribution and tumor detectability (*43*). The physiologic uptake of [^{18}F]AlF-NOTA-JR11 was significantly lower than that of [^{68}Ga]Ga-DOTATATE in the liver, spleen, adrenal gland, intestine, and pancreas but was higher in the blood and lungs. Furthermore, [^{18}F]AlF-NOTA-JR11 showed a significantly higher SUV_{max} in the liver lesions than did [^{68}Ga]Ga-DOTATATE, whereas no significant difference was found among the other groups. More primary and secondary lesions were detected with [^{18}F]AlF-NOTA-JR11 (226/227 lesions) than with [^{68}Ga]Ga-DOTATATE (160/227 lesions) because of the lower physiologic uptake by the digestive system. These findings indicate that [^{18}F]AlF-NOTA-JR11 could be a promising alternative to [^{68}Ga]Ga-DOTATATE, especially in lesions of the digestive system (*43*). However, novel high-affinity Al^{18}F-labeled SSTR2 antagonists might be warranted to further increase NET imaging sensitivity and to fully exploit the advantages of SSTR antagonists combined with the logistic advantages of ^{18}F.

FUTURE PERSPECTIVES

^{18}F-labeled SSA tracers are a promising alternative to ^{68}Ga-labeled SSAs. However, multiple questions about their use in clinical practice still remain unanswered. First, to our knowledge, no currently available clinical studies evaluated the interobserver agreement rate. Differences in interobserver concordance rates have already been described for ^{18}F-labeled prostate-specific membrane antigen tracers in comparison with their ^{68}Ga-labeled counterparts. Therefore, interobserver variability should also be assessed for ^{18}F-labeled SSA PET tracers. Second, several attempts have been made to evaluate the relationship between [^{68}Ga]Ga-DOTA SSA PET–derived quantitative parameters and treatment response after PRRT. Nevertheless, given the heterogeneous results of these studies, the predictive value of currently used ^{68}Ga-labeled SSA tracers is suboptimal in identifying patients who would benefit from PRRT (*44*). This limitation could possibly be overcome by the higher diagnostic accuracy of ^{18}F-labeled SSA tracers. Third, the impact on clinical management when using ^{18}F-labeled SSAs remains unclear and should be assessed in a multidisciplinary setting. Fourth, a more widespread use of ^{18}F-labeled SSAs may have a beneficial impact on patient outcomes. Improved lesion detection (e.g., by the higher spatial resolution and tumor-to-background ratio) could lead to a more accurate evaluation of disease extent, aiding physicians in making the right therapy choice. Finally, clinical data regarding the use of ^{18}F-labeled SSAs in other SSTR-expressing tumor subtypes (e.g., medullary thyroid cancer and small cell lung cancer) are currently lacking, and these entities need to be assessed in future studies.

CONCLUSION

In recent years, clinical studies have provided data that support the promising role of new ^{18}F-labeled SSA tracers. The beneficial physical properties of ^{18}F in combination with its higher production yield make these tracers an attractive alternative to ^{68}Ga-labeled tracers. Currently available clinical data on ^{18}F-labeled SSA tracers generally demonstrate higher in vivo stability, higher tumor-to-background ratios, better lesion detection, or a more favorable biodistribution than conventional [^{68}Ga]Ga-DOTA SSA tracers, indicating suitability for clinical use. Highly promising data for clinical use have been obtained for [^{18}F]SiTATE and [^{18}F]F-FET-βAG-TOCA. [^{18}F]AlF-NOTA-octreotide has been prospectively validated in a multicenter setting, with a favorable head-to-head comparison to [^{68}Ga]Ga-DOTA SSA tracers. ^{18}F-labeled SSTR agonist tracers should be implemented in guidelines and appropriate-use criteria for SSTR PET imaging, and future studies should focus on interobserver variability, impact on patient management, selection for peptide receptor radionuclide therapy, and therapy monitoring.

DISCLOSURE

Christophe Deroose is a senior clinical investigator from the Research Foundation–Flanders (FWO) and has been a consultant for Terumo, Ipsen, Sirtex, Bayer, and PSI CRO. Frederik Cleeren has been awarded an ERF nuclear medicine pilot research grant by the Neuroendocrine Tumor Research Foundation (NETRF). No other potential conflict of interest relevant to this article was reported.

REFERENCES

1. Hallet J, Law CHL, Cukier M, Saskin R, Liu N, Singh S. Exploring the rising incidence of neuroendocrine tumors: a population-based analysis of epidemiology, metastatic presentation, and outcomes. *Cancer.* 2015;121:589–597.
2. Bozkurt MF, Virgolini I, Balogova S, et al. Guideline for PET/CT imaging of neuroendocrine neoplasms with ^{68}Ga-DOTA-conjugated somatostatin receptor targeting peptides and ^{18}F-DOPA. *Eur J Nucl Med Mol Imaging.* 2017;44:1588–1601.
3. Sampedro-Núñez M, Luque RM, Ramos-Levi AM, et al. Presence of sst5TMD4, a truncated splice variant of the somatostatin receptor subtype 5, is associated to features of increased aggressiveness in pancreatic neuroendocrine tumors. *Oncotarget.* 2016;7:6593–6608.
4. Günther T, Tulipano G, Dournaud P, et al. International union of basic and clinical pharmacology. CV. Somatostatin receptors: structure, function, ligands, and new nomenclature. *Pharmacol Rev.* 2018;70:763–835.
5. Reubi JC, Laissue J, Krenning E, Lamberts SWJ. Somatostatin receptors in human cancer: incidence, characteristics, functional correlates and clinical implications. *J Steroid Biochem Mol Biol.* 1992;43:27–35.
6. Deroose CM, Hindié E, Kebebew E, et al. Molecular imaging of gastroenteropancreatic neuroendocrine tumors: current status and future directions. *J Nucl Med.* 2016;57:1949–1956.
7. Volante M, Rosas R, Allìa E, et al. Somatostatin, cortistatin and their receptors in tumours. *Mol Cell Endocrinol.* 2008;286:219–229.
8. Reubi JC. Somatostatin and other peptide receptors as tools for tumor diagnosis and treatment. *Neuroendocrinology.* 2004;80:51–56.
9. Nedrow JR, White AG, Modi J, Nguyen K, Chang AJ, Anderson CJ. Positron emission tomographic imaging of copper 64- and gallium 68-labeled chelator conjugates of the somatostatin agonist Tyr 3-octreotate. *Mol Imaging.* 2014;13:1–13.
10. Krenning EP, Breeman WAP, Kooij PPM, et al. Localisation of endocrine-related tumours with radioiodinated analogue of somatostatin. *Lancet.* 1989;1:242–244.
11. Krenning EP, Bakker WH, Kooij PPM, et al. Somatostatin receptor scintigraphy with indium-111-DTPA-D-Phe-1-octreotide in man: metabolism, dosimetry and comparison with iodine-123-Tyr-3-octreotide. *J Nucl Med.* 1992;33:652–658.
12. Smit Duijzentkunst DAS, Kwekkeboom DJ, Bodei L. Somatostatin receptor 2-targeting compounds. *J Nucl Med.* 2017;58(suppl 2):54S–60S.
13. Ambrosini V, Fani M, Fanti S, Forrer F, Maecke HR. Radiopeptide imaging and therapy in Europe. *J Nucl Med.* 2011;52(suppl 2):42S–55S.
14. Gabriel M, Decristoforo C, Donnemiller E, et al. An intrapatient comparison of ^{99m}Tc-EDDA/HYNIC-TOC with ^{111}In-DTPA-octreotide for diagnosis of somatostatin receptor-expressing tumors. *J Nucl Med.* 2003;44:708–716.
15. Poletto G, Cecchin D, Sperti S, Filippi L, Realdon N, Evangelista L. Head-to-head comparison between peptide-based radiopharmaceutical for PET and SPECT in the evaluation of neuroendocrine tumors: a systematic review. *Curr Issues Mol Biol.* 2022;44:5516–5530.
16. Pauwels E, Cleeren F, Bormans G, Deroose C. Somatostatin receptor PET ligands the next generation for clinical practice. *Am J Nucl Med Mol Imaging.* 2018;8:311–331.
17. Meisetschläger G, Poethko T, Stahl A, et al. Gluc-Lys([^{18}F]FP)-TOCA PET in patients with SSTR-positive tumors: biodistribution and diagnostic evaluation compared with [^{111}In]DTPA-octreotide. *J Nucl Med.* 2006;47:566–573.
18. Seemann MD. Detection of metastases from gastrointestinal neuroendocrine tumors: prospective comparison of ^{18}F-TOCA PET, triple-phase CT, and PET/CT. *Technol Cancer Res Treat.* 2007;6:213–220.
19. Wieder H, Beer AJ, Poethko T, et al. PET/CT with Gluc-Lys-([^{18}F]FP)-TOCA: correlation between uptake, size and arterial perfusion in somatostatin receptor positive lesions. *Eur J Nucl Med Mol Imaging.* 2008;35:264–271.
20. Astner ST, Bundschuh RA, Beer AJ, et al. Assessment of tumor volumes in skull base glomus tumors using Gluc-Lys[^{18}F]-TOCA positron emission tomography. *Int J Radiat Oncol Biol Phys.* 2009;73:1135–1140.
21. Dubash SR, Nicholas K, Mapelli P, et al. Clinical translation of a click-labeled ^{18}F-octreotate radioligand for imaging neuroendocrine tumors. *J Nucl Med.* 2016;57:1207–1213.
22. Dubash SR, Barwick T, Mauri FA, et al. [^{18}F]FET-βAG-TOCA versus [^{68}Ga]DOTATATE PET/CT in functional imaging of neuroendocrine tumours [abstract]. *J Clin Oncol.* 2018;36(suppl):e24193.
23. Ćorović A, Wall C, Nus M, et al. Somatostatin receptor PET/MR imaging of inflammation in patients with large vessel vasculitis and atherosclerosis. *J Am Coll Cardiol.* 2023;81:336–354.
24. Tshibangu T, Cawthorne C, Serdons K, et al. Automated GMP compliant production of [^{18}F]AlF-NOTA-octreotide. *EJNMMI Radiopharm Chem.* 2020;5:4.
25. Long T, Yang N, Zhou M, et al. Clinical application of ^{18}F-AlF-NOTA-octreotide PET/CT in combination with ^{18}F-FDG PET/CT for imaging neuroendocrine neoplasms. *Clin Nucl Med.* 2019;44:452–458.
26. Hou J, Long T, Yang N, et al. Biodistribution of ^{18}F-AlF-NOTA-octreotide in different organs and characterization of uptake in neuroendocrine neoplasms. *Mol Imaging Biol.* 2021;23:827–835.
27. Hofman MS, Eddie Lau WF, Hicks RJ. Somatostatin receptor imaging with ^{68}Ga-DOTATATE PET/CT: clinical utility, normal patterns, pearls, and pitfalls in interpretation. *Radiographics.* 2015;35:500–516.
28. Pauwels E, Cleeren F, Tshibangu T, et al. Al^{18}F-NOTA-octreotide: first comparison with ^{68}Ga-DOTATATE in a neuroendocrine tumour patient. *Eur J Nucl Med Mol Imaging.* 2019;46:2398–2399.
29. Pauwels E, Cleeren F, Tshibangu T, et al. [^{18}F]AlF-NOTA-octreotide PET imaging: biodistribution, dosimetry and first comparison with [^{68}Ga]Ga-DOTATATE in neuroendocrine tumour patients. *Eur J Nucl Med Mol Imaging.* 2020;47:3033–3046.
30. Hou J, Long T, He Z, et al. Evaluation of ^{18}F-AlF-fetNOTA-octreotide for imaging neuroendocrine neoplasms: comparison with ^{68}Ga-DOTATATE PET/CT. *EJNMMI Res.* 2021;11:55.
31. Pauwels E, Cleeren F, Tshibangu T, et al. 18F-AlF-NOTA-octreotide outperforms 68Ga-DOTATATE/NOC PET in neuroendocrine tumor patients: results from a prospective, multicenter study. *J Nucl Med.* 2023;64:632–638.
32. Haeger A, Soza-Ried C, Kramer V, et al. Al[^{18}F]F-NOTA-octreotide is comparable to [^{68}Ga]Ga-DOTA-TATE for PET/CT imaging of neuroendocrine tumours in the Latin-American population. *Cancers (Basel).* 2023;15:439–450.
33. Hou J, Long T, Yang Y, Chen D, Hu S. The potential prognostic value of dual-imaging PET parameters based on ^{18}F-FDG and ^{18}F-OC for neuroendocrine neoplasms. *Mol Imaging.* 2022;2022:6511179.
34. Lindner S, Simmet M, Gildehaus FJ, et al. Automated production of [^{18}F]SiTATE on a Scintomics GRP^{TM} platform for PET/CT imaging of neuroendocrine tumors. *Nucl Med Biol.* 2020;88–89:86–95.
35. Wängler C, Beyer L, Bartenstein P, Wängler B, Schirrmacher R, Lindner S. Favorable SSTR subtype selectivity of SiTATE: new momentum for clinical [^{18}F]SiTATE PET. *EJNMMI Radiopharm Chem.* 2022;7:22.
36. Ilhan H, Todica A, Lindner S, et al. First-in-human ^{18}F-SiFAlin-TATE PET/CT for NET imaging and theranostics. *Eur J Nucl Med Mol Imaging.* 2019;46:2400–2401.
37. Ilhan H, Lindner S, Todica A, et al. Biodistribution and first clinical results of ^{18}F-SiFAlin-TATE PET: a novel ^{18}F-labeled somatostatin analog for imaging of neuroendocrine tumors. *Eur J Nucl Med Mol Imaging.* 2020;47:870–880.
38. Beyer L, Gosewisch A, Lindner S, et al. Dosimetry and optimal scan time of [^{18}F]SiTATE-PET/CT in patients with neuroendocrine tumours. *Eur J Nucl Med Mol Imaging.* 2021;48:3571–3581.
39. Eschbach RS, Hofmann M, Späth L, et al. Comparison of somatostatin receptor expression in patients with neuroendocrine tumours with and without somatostatin analogue treatment imaged with [^{18}F]SiTATE. *Front Oncol.* 2023;13:992316.
40. Unterrainer M, Unterrainer L, Kunte SC, et al. Next generation PET/CT imaging in meningioma: first clinical experiences using the novel SSTR-targeting peptide ^{18}F-SiTATE [abstract]. *J Nucl Med.* 2022;63(suppl 2):2289.
41. Unterrainer M, Lindner S, Beyer L, et al. PET imaging of meningioma using the novel SSTR-targeting peptide ^{18}F-SiTATE. *Clin Nucl Med.* 2021;46:667–668.
42. Nicolas GP, Schreiter N, Kaul F, et al. Sensitivity comparison of ^{68}Ga-OPS202 and ^{68}Ga-DOTATOC PET/CT in patients with gastroenteropancreatic neuroendocrine tumors: a prospective phase II imaging study. *J Nucl Med.* 2018;59:915–921.
43. Xie Q, Liu T, Ding J, et al. Synthesis, preclinical evaluation, and a pilot clinical imaging study of [^{18}F]AlF-NOTA-JR11 for neuroendocrine neoplasms compared with [^{68}Ga]Ga-DOTA-TATE. *Eur J Nucl Med Mol Imaging.* 2021;48:3129–3140.
44. Ahmadi Bidakhvidi A, Goffin K, Dekervel J, et al. Peptide receptor radionuclide therapy targeting the somatostatin receptor: basic principles, clinical applications and optimization strategies. *Cancers (Basel).* 2021;14:129.
45. Vermeulen K, Vandamme M, Bormans G, Cleeren F. Design and challenges of radiopharmaceuticals. *Semin Nucl Med.* 2019;49:339–356.